Sulfur and chlorine solubility in Mt. Unzen rhyodacitic melt at 850 °C and 200 MPa

R.E. Botcharnikov[a,*], H. Behrens[a], F. Holtz[a], J. Koepke[a], H. Sato[b]

[a]*Institut für Mineralogie, Universität Hannover, Callinstr. 3, D-30167, Hannover, Germany*
[b]*Department of Earth and Planetary Sciences, Kobe University, Kobe, 657-8501 Japan*

Abstract

The solubilities of S and Cl have been determined at 850 °C, 200 MPa, and fO_2 ~NNO in a rhyodacitic melt of the Unzen volcano in equilibrium with a fluid phase of mixed composition (H–O–Cl–S). The partitioning of Cl between silicate melt and fluid shows a strong deviation from ideal behavior. The Cl content of melts coexisting with fluids containing up to 50 mol% Cl is approximately 0.85 wt.%. With the addition of sulfur, the Cl concentration decreases by 0.2 wt.% Cl (2 wt.% S added in the system; ~50 mol% Cl in fluid). This effect is most probably explained by a more ideal mixing of the Cl-bearing species in S-bearing fluids. However, changes of melt composition with the addition of S (depletion of iron) can also influence Cl solubility. The solubility of sulfur in the melt is a complex function of the activity of fluid components, the FeO_{tot} content of the melt, and the speciation of S. With increasing S content in the system from 0 to 2 wt.% S, the amount of pyrrhotite (Pyr) increases (up to 2.2 vol.%), the FeO_{tot} content of the melt decreases (from 2.8 to 0.9 wt.% FeO_{tot}), and S solubility increases slightly (up to 100 ppm). At the investigated conditions in the Cl-bearing systems, S solubilities up to 200 ppm have been determined, indicating that the addition of Cl to the system enhances S solubility.

The influence of Cl on the solubility of S can be related to nonideal mixing in the fluid, in particular, the increase in activity of S-bearing fluid species and a decrease of H_2S/SO_2 ratios in the fluid. The first effect leads to higher solubility of sulfide in the melt and the second one favors the dissolution of additional sulfate in the silicate melt at studied conditions.
© 2004 Elsevier B.V. All rights reserved.

Keywords: Sulfur; Chlorine; Mixed fluid; Solubility; Silicate melt; Magma degassing; Unzen volcano

1. Introduction

Volcanic gases contain mainly H_2O, CO_2, SO_2, H_2S, HCl, and, to a lower extent, HF (e.g., Giggenbach, 1996; Symonds et al., 1994). At the onset of magma degassing, all these volatiles will be involved in different extents to the formation of a multi-

---

* Corresponding author. Fax: +49 511 762 3045.

E-mail address: R.Botcharnikov@mineralogie.uni-hannover.de (R.E. Botcharnikov).

component fluid phase due to different solubilities of the volatiles in the melt and due to the mixing properties of the fluid phase. Thus, modeling the degassing of natural magmas requires the understanding of the solubilities of volatiles in melts in equilibrium with complex mixed fluids.

Although sometimes present in small amounts when compared with water, C-, Cl-, and S-bearing species play an important role in magmatic and degassing processes. However, there are very few data concerning the solubility of carbon, sulfur, and chlorine in hydrous silicate melts in equilibrium with multicomponent fluids (containing C, Cl, and S). The lack of solubility data is related to difficulties in controlling the fugacities of volatiles in the experiments. Moreover, the interpretation of experimental results in such complex systems containing multicomponent fluids requires the knowledge on the properties of simple systems containing pure and binary fluids. In the past decade, our understanding of such simple fluid-melt systems has been largely improved, especially for felsic melts (e.g., Carroll and Webster, 1994; Holloway and Blank, 1994; Scaillet et al., 1998; Tamic et al., 2001; Webster and De Vivo, 2002; Moretti et al., 2003; Scaillet and Pichavant, 2003; Behrens et al., in press). Investigations on volatile solubilities in melts coexisting with C–O–H–Cl-bearing fluids suggest that the increasing abundance of CO_2 in the aqueous fluid has either insignificant (Webster, 1997) or small positive effect on the solubility of chlorine in the melt, probably due to a decrease in the mean dielectric constant of the fluid phase and an increase in activity of chlorine in the fluid (Webster and Holloway, 1988). This is related to an enlargement of the *P-T-X* range of the immiscibility gap in H_2O–salt fluid systems with the addition of CO_2 (e.g., Joyce and Holloway, 1993; Duan et al., 1995, 2003; Shmulovich et al., 1995; Shmulovich and Graham, 2004).

To our knowledge, the solubility of volatiles in melts coexisting with H–O–Cl–S-bearing fluids has not been investigated systematically so far. The behavior of such mixed fluids is of increasing interest because the concentrations and ratios of sulfur and chlorine volatile compounds in magmas and volcanic gases are often used in volcanology to reconstruct the evolution of magmatic systems (e.g., Metrich et al., 1993; Symonds et al., 1994; Francis et al., 1995; Self and King, 1996; Thordarson et al., 1996; Mori et al., 1993; Mori and Notsu, 1997; Harms and Schmincke, 2000; De Hoog et al., 2001; Edmonds et al., 2001; Webster et al., 2001; Aiuppa et al., 2002; Davis et al., 2003). As a step towards natural fluid-melt systems, we conducted the first experiments on the solubility of sulfur and chlorine in a rhyodacitic melt in equilibrium with mixed aqueous fluids at P=200 MPa, T=850 °C, and $\log fO_2$=NNO. Such melt composition and conditions were chosen to understand the behavior of volatiles during recent eruption of Unzen volcano, Japan.

2. Experiment

2.1. Starting materials

The starting material is a synthetic analogue of a rhyodacitic silicate melt (Table 1), which corresponds to the groundmass composition of the magma erupted by Unzen volcano in 1991–1995 (Nakada and Motomura, 1999; Sato et al., 1999). It was prepared from a mixture of oxides (SiO_2, TiO_2, Al_2O_3, Fe_2O_3, MnO, and MgO) and carbonates ($CaCO_3$, Na_2CO_3, and K_2CO_3), ground in a rotary mortar. The powder was melted for 2 h in Pt crucibles at 1600 °C, 1 atm in air ($\log fO_2$=−0.68). The melt was quenched to glass by placing the crucible into a water bath. Then, the glass was ground again in the agate mortar and remelted for 0.5 h to improve the homogeneity of the batch. The homogeneity of the silicate glass was verified by electron microprobe (Table 1). The glass was finally crushed in the mortar and sieved to the

Table 1
Chemical composition of starting rhyodacitic glass in wt.%

SiO₂	TiO₂	Al₂O₃	FeO_tot	MnO	MgO	CaO	Na₂O	K₂O	Total	#Mg[a]	A/CNK[b]
69.95	0.50	14.21	3.57	0.12	1.44	4.05	3.16	2.75	99.75	0.42	0.915

[a] #Mg=Mg/(Mg+Fe), where Fe is a total molar amount of iron in silicate glass.
[b] Molar $Al_2O_3/(CaO+Na_2O+K_2O)$ ratio.

grain sizes of <100 and 100–200 μm. The two fractions were mixed together in a volume ratio ~1:1 to minimize the free volume in the experimental capsules and to reduce the incorporation of atmospheric nitrogen into the charge. The obtained starting glass powder was stored in a desiccator.

2.2. Experimental method

Fifty milligrams of powdered silicate glass was mixed with various amounts of elemental sulfur powder (0–1 mg) and loaded in 15-mm-long (inner diameter of 2.8 mm) gold capsules. Five microliters of pure water or aqueous HCl solution (0.9–33 wt.% HCl) was added to the charge in the capsules and quantified by measuring the weight gain. The initial amount of Cl in the 33 wt.% HCl solution was verified using a Mettler DL25 Titrator. The amounts of S, Cl, and water added to the dry silicate glass are listed in Table 2 for each experiment. The amounts of S were chosen so that the fractions of S in relation to the silicate glass are close to 0.5, 1, and 2 wt.%. Capsules were welded shut and heated overnight in an oven at 110 °C to homogenize fluid distribution inside the capsule and check for leaks.

Experiments were carried out in conventional horizontal cold seal pressure vessels (CSPV) made of an alloy containing mainly Ni. The vessels were pressurized with water. Temperature was controlled with an external Ni–CrNi thermocouple (vessels are calibrated for temperature) and the variations were less than 5 °C. The accuracy in temperature is estimated to be ±10 °C. Pressure was measured with a strain gauge manometer and controlled manually. The pressure variations were 5 MPa. All experimental runs were quenched isobarically with a flux of compressed air. The oxygen fugacity inside CSPVs was buffered through the reaction of water with the Ni/NiO solid oxygen buffer (charged as a mixture of Ni and NiO powders). The use of water as pressure medium and the Ni-bearing alloy of the vessel allowed to keep the fO_2 conditions at the Ni/NiO buffer for long duration in the CSPVs. The constant fO_2 value means also constant fugacity of hydrogen in CSPV due to the reaction of buffer assemblage with water. Furthermore, the fH_2 is also fixed inside the experimental capsules due to the diffusion of hydrogen through the capsule walls at high temperature. Thus, the use of NNO external buffer imposes the constant hydrogen fugacity in the experimental charges which governs, in turn, redox reactions among melt, mineral, and fluid phases.

Table 2
Starting mass relations in the experimental runs

Run number	Mass glass (mg)	Mass HCl (mg)	Mass S (mg)	Mass Cl[a] (mg)	Mass H$_2$O[a] (mg)	Bulk added Cl (wt.%)	Bulk added S (wt.%)
S-100	49.78	–	0.30	–	4.94	0.00	0.55
S-101	49.93	–	0.69	–	4.95	0.00	1.24
S-102	49.93	–	1.07	–	4.96	0.00	1.91
ClS-88	49.89	4.95	0.26	0.05	4.90	0.09	0.47
Cl-51	50.78	4.99	–	0.14	4.85	0.25	0.00
ClS-79	49.86	5.01	0.25	0.14	4.87	0.25	0.45
ClS-80	49.93	4.99	0.50	0.14	4.85	0.25	0.90
ClS-78	50.25	5.03	1.00	0.14	4.89	0.25	1.78
Cl-52	50.70	5.08	–	0.28	4.80	0.50	0.00
ClS-104	49.90	5.05	0.56	0.28	4.77	0.50	1.01
Cl-53	50.37	5.19	–	0.58	4.61	1.04	0.00
ClS-103	49.60	5.24	0.25	0.61	4.63	1.11	0.45
ClS-76	50.37	4.63	0.51	0.52	4.11	0.94	0.92
ClS-75	50.32	5.14	1.00	0.57	4.57	1.01	1.77
Cl-72	50.01	5.25	–	1.76	3.49	3.18	0.00
ClS-74	49.84	4.62	0.25	1.55	3.07	2.83	0.46
ClS-105	48.81	5.78	0.55	1.94	3.84	3.52	1.00
ClS-73	50.12	5.38	1.00	1.80	3.58	3.19	1.77

[a] Calculated from the Cl and H$_2$O concentrations in the HCl solution.

Table 3

Mineral assemblages and composition of silicate glass (wt.%$\pm 1\sigma$) after experiments at 850 °C and 200 MPa

Run number[a]	n[b]	SiO_2	TiO_2	Al_2O_3	FeO*	MnO	MgO	CaO
S-100								
0.0% Cl	4	65.79±0.12	0.47±0.03	13.76±0.16	2.50±0.11	0.12±0.10	0.70±0.09	3.06±0.18
0.55% S								
S-101								
0.0% Cl	6	65.72±0.80	0.47±0.05	14.22±0.40	1.93±0.26	0.08±0.10	0.72±0.04	3.06±0.21
1.24% S								
S-102								
0.0% Cl	13	66.56±0.88	0.47±0.05	13.89±0.25	1.70±0.25	0.10±0.07	0.67±0.05	3.00±0.10
1.91% S								
ClS-88								
0.09% Cl	10	65.12±0.12	0.47±0.04	13.44±0.16	2.47±0.11	0.02±0.09	0.68±0.09	3.29±0.18
0.47% S								
Cl-51								
0.25% Cl	16	66.69±0.23	0.36±0.02	14.02±0.14	2.54±0.24	0.11±0.04	0.53±0.05	3.12±0.12
0.0% S 16								
ClS-79								
0.25% Cl	19	67.23±0.46	0.43±0.03	13.82±0.17	2.33±0.18	0.11±0.06	0.67±0.04	3.08±0.07
0.45% S								
ClS-80								
0.25% Cl	18	67.94±0.49	0.44±0.02	13.91±0.16	1.92±0.13	0.10±0.05	0.70±0.04	3.01±0.12
0.90% S								
ClS-78								
0.25% Cl	15	68.26±0.53	0.47±0.02	13.77±0.13	1.13±0.12	0.10±0.07	0.70±0.03	2.86±0.08
1.78% S								
Cl-52								
0.50% Cl	16	66.09±0.30	0.40±0.02	14.03±0.16	2.78±0.16	0.13±0.05	0.69±0.05	3.37±0.09
0.0% S								
ClS-104								
0.50% Cl	9	65.99±0.35	0.46±0.05	13.81±0.27	2.15±0.16	0.12±0.08	0.90±0.10	3.35±0.15
1.01% S								
Cl-53								
1.04% Cl	16	66.01±0.36	0.45±0.02	14.07±0.13	2.72±0.13	0.11±0.05	0.79±0.04	3.64±0.10
0.0% S								
ClS-103								
1.11% Cl	10	65.95±0.35	0.49±0.05	13.70±0.17	2.41±0.20	0.09±0.10	0.93±0.06	3.66±0.18
0.45% S								
ClS-76								
0.94% Cl	16	68.72±0.43	0.43±0.02	13.39±0.14	1.69±0.14	0.10±0.05	0.66±0.04	2.95±0.09
0.92% S								
ClS-75								
1.01% Cl	17	69.93±0.32	0.46±0.03	13.23±0.12	0.87±0.11	0.06±0.05	0.69±0.04	2.87±0.08
1.77% S								
Cl-72								
3.18% Cl	15	68.65±0.25	0.51±0.02	13.33±0.15	2.30±0.17	0.08±0.05	0.86±0.22	3.14±0.10
0.0% S								
ClS-74								
2.83% Cl	16	69.28±0.36	0.51±0.01	13.28±0.12	1.96±0.12	0.08±0.05	0.86±0.03	3.10±0.09
0.46% S								
ClS-105								
3.52% Cl	8	67.34±0.69	0.47±0.05	13.87±0.24	0.92±0.14	0.06±0.08	1.29±0.09	3.53±0.08
1.00% S								
ClS-73								
3.19% Cl	17	69.57±0.29	0.50±0.03	13.39±0.09	0.86±0.09	0.09±0.05	1.09±0.04	3.02±0.09
1.77% S								

Na$_2$O	K$_2$O	Cl	S	Total	H$_2$O[c]	#Mg[d]	A/CNK[e]	Determined phases[f,g]
2.88±0.03	2.55±0.09	–	0.006±0.001	91.83±0.23	6.8±0.5	0.33	1.053	Gl (92.8), Hb (6.6), Pyr (0.6)
2.92±0.36	2.73±0.14	–	0.010±0.005	91.83±1.78	6.5±1.8	0.40	1.067	Gl (92.0) Hb (6.8), Pyr (1.1), Pl (trace amounts)
2.87±0.60	2.69±0.14	–	0.010±0.004	91.97±1.22	5.9±1.2	0.41	1.061	Gl (92.1), Hb (5.3), Pyr (1.7), Pl (1.0)
2.78±0.04	2.60±0.09	0.084±0.005	0.006±0.002	91.00±0.31	7.4±0.5	0.33	1.005	Gl (95.0), Hb (4.1), Pyr (0.5), Pl (0.3)
2.62±0.18	2.72±0.07	0.219±0.013	–	92.93±0.49	6.5±0.5	0.27	1.085	Gl (91.5), Opx+Hb (5.8), Pl (2.7)
2.43±0.21	2.76±0.09	0.225±0.008	0.013±0.004	93.10±0.89	7.3±0.9	0.34	1.098	Gl (91.2), Hb (4.8), Pl (3.6), Pyr (0.4)
2.54±0.23	2.79±0.07	0.226±0.007	0.016±0.004	93.60±0.83	6.8±0.8	0.39	1.098	Gl (92.1), Pl (3.5), Hb (3.2), Pyr (1.2)
2.41±0.51	2.87±0.07	0.220±0.018	0.014±0.006	92.81±1.00	7.6±1.0	0.53	1.122	Gl (88.2), Pl (5.6), Hb (4.1), Pyr (2.0)
2.66±0.11	2.61±0.07	0.459±0.014	–	93.20±0.49	6.2±0.5	0.31	1.053	Gl (94.6), Opx+Hb (3.8), Pl (1.5)
2.93±0.22	2.66±0.07	0.361±0.041	0.016±0.006	92.74±0.36	6.8±0.5	0.43	1.001	Gl (95.5), Hb (3.6), Pyr (0.9)
2.60±0.22	2.55±0.08	0.655±0.015	–	93.58±0.37	5.9±0.5	0.34	1.030	Gl (96.7), Opx+ Hb(2.3), Pl (1.0)
2.80±0.25	2.42±0.14	0.660±0.025	0.014±0.007	93.15±0.58	6.3±0.6	0.41	0.987	Gl (97.4), Hb (2.2), Pyr (0.4)
2.45±0.19	2.83±0.08	0.567±0.020	0.018±0.006	93.81±0.63	6.6±0.6	0.41	1.075	Gl (90.7), Hb (4.2), Pl (4.0), Pyr (1.1)
2.51±0.16	2.85±0.07	0.511±0.021	0.017±0.005	94.00±0.46	6.4±0.5	0.59	1.064	Gl (86.9), Pl (6.1), Hb (4.8), Pyr (2.2)
2.33±0.14	2.48±0.09	0.854±0.025	–	94.54±0.42	5.9±0.5	0.40	1.090	Gl (92.6), Pl (4.2), Opx (3.1)
2.32±0.11	2.51±0.08	0.793±0.018	0.016±0.006	94.70±0.48	5.7±0.5	0.44	1.091	Gl (92.2), Pl (4.6), Opx (2.7), Pyr (0.4)
2.43±0.13	2.03±0.10	0.805±0.037	0.018±0.010	92.77±0.82	6.9±0.8	0.71	1.100	Gl (98.0), Hb (1.4), Pyr (0.7)
2.28±0.08	2.43±0.07	0.658±0.032	0.020±0.005	93.89±0.33	6.5±0.5	0.69	1.128	Gl (90.7), Pl (4.3), Opx (3.7), Pyr (1.4)

All experiments were performed at T=850 °C and P=200 MPa. Such conditions are close to those prevailing in the magma chamber of Unzen volcano after magma mixing (e.g., Venezky and Rutherford, 1999; Sato et al., 1999; Holtz et al., in press). At those conditions and for the investigated melt composition, the amount of added aqueous fluid was enough to ensure fluid saturation in all runs.

The duration of the experimental runs was 120 ± 5 h. In previous studies, run duration of 2–5 days was found to be sufficient to achieve equilibrium in hydrous Cl- or S-bearing felsic magmas at conditions similar to our experiments (e.g., Carroll and Rutherford, 1987; Malinin et al., 1989; Shinohara et al., 1989; Luhr, 1990; Metrich and Rutherford, 1992; Webster, 1992; Signorelli and Carroll, 2000).

3. Analytical methods

3.1. Electron microprobe

The run products were composed of minerals (plagioclase, Pl; orthopyroxene, Opx; hornblende, Hb; pyrrhotite, Pyr) and glass (Gl). A Cameca SX-100 electron microprobe was used to identify the minerals and to analyze the compositions of the glasses. Glass analyses were conducted with 15 kV acceleration potential, 6-nA beam current, a defocused electron beam (10–20 μm diameter), and peak counting times of 2–5 s (for major elements). Sodium and potassium were analyzed first for 2 s to minimize their migration. The alkali loss was determined in sample Cl-72 as a function of counting time (from 2 to 90 s). The obtained curve (counts/second vs. time) was fitted and extrapolated to the zero time. The difference between Na_2O and K_2O concentrations calculated at zero-time and those determined after 2-s measurements is less than the analytical error given in Table 3 (this error

corresponds to the one σ deviation of the analyses). Thus, the alkali loss was neglected at our analytical conditions.

Pyrrhotite crystals were analyzed at 15 nA beam current and focused beam. For the sulfur analyses, the wavelength of the SKα radiation was estimated in silicate glasses (Carroll and Rutherford, 1988) and pyrrhotites, and the peak position was compared with the standards (BaSO$_4$ and ZnS). Due to low sulfur concentration in the glasses, the observed peaks were broad and the height of the peaks was low. However, the SKα peak position in the glasses was found to be close to that of sulfur bound as sulfide, which is reasonable at fO_2 buffered with NNO (Carroll and Rutherford, 1988). Chlorine and sulfur were measured as the last elements, and the counting times for S and Cl were 100 to 200 s and 60 to100 s, respectively. Using standards for S and Cl (NaCl), multiple measurements were made for each sample (5–20 analyses) to reduce possible analytical errors and to check for homogeneity. The relative analytical errors for sulfur determination are high mostly due to the low sulfur concentrations, slightly above the detection limit of 40 ppm. Chlorine can be measured more precisely because its concentration in the melt is about one order of magnitude higher than the detection limit of 300 ppm. The microprobe analyses were not calibrated against additional standard silicate glasses with known amount of chlorine and sulfur. However, the analytical conditions were identical for all measured glasses. It implies that, even if the absolute values of Cl and S concentration may have a systematic error, the relative changes are measured accurately.

3.2. Analyses of backscattered electron (BSE) images

The analyses of backscattered electron (BSE) images of the experimental products have been used

---

Notes to Table 3:

[a] Sample number and bulk concentrations of Cl and S (wt.%) added to the system.

[b] Number of electron microprobe analyses.

[c] Water content of the melt (wt.%) determined using the by-difference method after microprobe analyses.

[d] #Mg=Mg/(Mg+Fe), where Fe is the total molar amount of iron in glasses.

[e] Molar Al_2O_3/(CaO+Na_2O+K_2O) ratio of experimental glasses.

[f] Gl=glass; Opx=orthopyroxene; Hb=hornblende; Pl=plagioclase; Pyr=pyrrhotite.

[g] Modal proportions of phases (vol.%) determined by image analysis (see text).

to determine the modal proportions of glass and mineral phases in our samples. It was possible to distinguish all mineral phases, except for Opx and Hb because these phases have almost identical brightness in backscattered electrons images. Therefore, in this study, the amount of Opx and Hb was determined as a whole (Opx+Hb). Because crystals in the experimental products are not oriented preferentially and are distributed homogeneously (see Fig. 1), the modal proportions determined from a two-dimensional analysis can be extrapolated to the volume of the sample. Three or four BSE images with a size of 300×300 or/ and 600×600 μm have been processed for each sample to evaluate possible errors of this method. The reproducibility of the percentage volume of silicate glass in the charges was always within ±3 vol.%, in most cases, even within ±1 vol.%. The relative error of glass proportions resulting from the reproducibility mentioned above is 3%. In contrast, the relative error of the proportions of solid phases is higher because of their small proportions in the run products [at most ±74% for Pl, ±44% for (Opx+Hb), and ±80% for Pyr].

3.3. Mass balance calculations

The modal proportions of glass and mineral phases were transferred into mass proportions, taking into account the densities of the phases (using values after Deer et al., 1992). This allows mass balance calculation of the composition of the fluid phase, which was in equilibrium with the silicate melt. The mass balance calculations were necessary because with the experimental strategy used in this study, the exact composition of the fluid phase cannot be determined directly (small amounts of fluid were used to minimize the effect of incongruent dissolution of the silicate components in the fluid) and because the fluid phase composition added to the starting dry glass is different from that in the run products due to differences in solubilities for H_2O, Cl, and S.

The water content of the melt was determined using the "by-difference method". In doing so, we assume that the difference to 100% in electron microprobe analysis is caused exclusively by the presence of unmeasured H_2O. To improve the method, the difference values were corrected using a hydrous
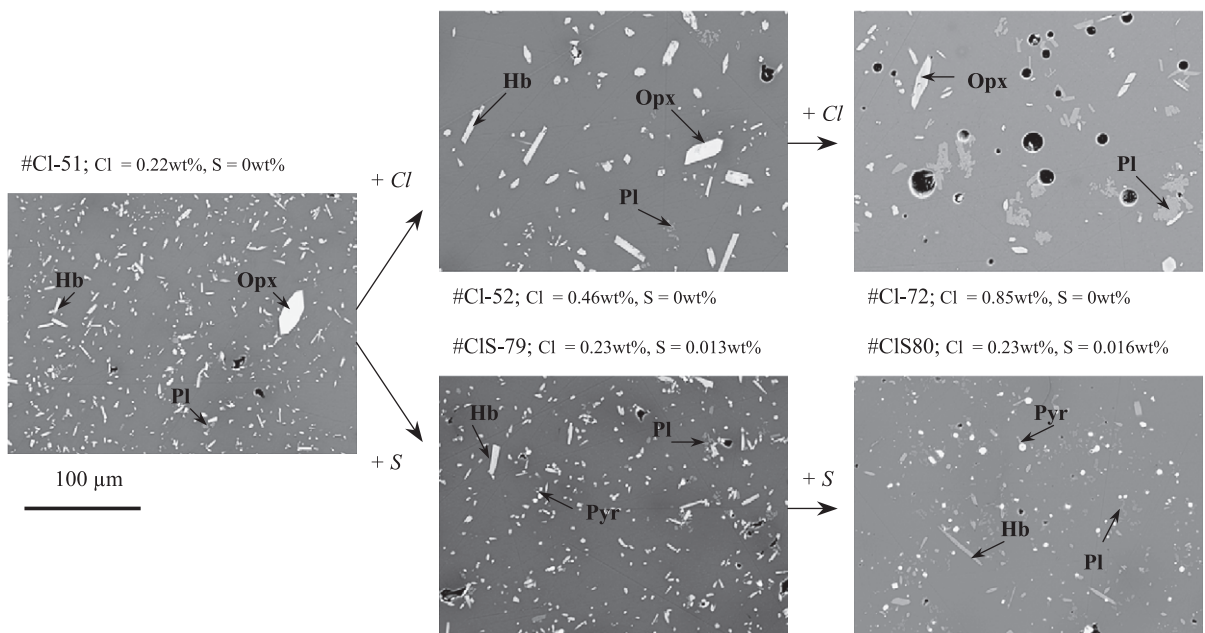

Fig. 1. The backscattered electron images of experimental products (samples number Cl-51, Cl-52, Cl-72, ClS-79, and ClS-80) illustrating changes in the proportions of melt and crystals, in mineral assemblages, and in the size of the minerals with increasing contents of chlorine and sulfur in the melt (indicated in wt.% in labels). See also text and Table 3 for description and modal proportions of phases.

rhyodacitic glass (5.9 wt.% H_2O) for which the water content was measured by KFT analysis. The error of the by-difference method is large due to high uncertainty in counting statistics of electron microprobe for major element composition and the typical error is more than ± 0.5 wt.% (e.g., Devine et al., 1995). Although the error of the total in our microprobe analyses is lower for some samples (Table 3), we assume that a minimum error of ± 0.5 wt.% has to be considered in general for this method.

Sulfur is present in melt, fluid, and pyrrhotite. The S contents of the melt and pyrrhotite were measured by electron microprobe. Thus, knowing the proportions of melt and pyrrhotite, the concentration of S in both phases, and the amount of bulk added sulfur, it is possible to calculate the mass of S contained in the fluid phase. This calculation is valid if it is assumed that no sulfur is incorporated into the capsule. In this study, the sulfur content in the capsule was not determined. The analyses of S in Au capsules after the experiments performed at 900 °C, similar fO_2, 1 wt.% S added, and run duration of 5 days show that some sulfur can be incorporated into the capsule but that the distribution of S is strongly heterogeneous (with maximum values up to 500 ppm; F. Parat, personal communication). Because of this heterogeneous S distribution, it is impossible to calculate the amount of S dissolved in the noble metal. In the discussion of our results, the loss of sulfur into the capsule was not considered, implying that the calculated absolute S concentrations in the fluid are overestimated. Nevertheless, the results can be used to discuss the data as a function of relative variations of fluid compositions.

Chlorine is partitioned between melt and fluid(s) only. No Cl-bearing mineral phase was found at the studied conditions. The concentration of Cl incorporated into amphiboles is usually <0.1 wt.% (see also Sato et al., in press) contributing less than five relative percent to the total Cl content of the system. Hence, it was neglected from mass balance calculations. Although we have no analytical constraints on the fluid phase relations, fluid immiscibility (i.e., a H_2O-rich fluid coexisting with a Cl-rich brine) is not expected at our experimental conditions for the H_2O–Cl-bearing system (according to the data for the H_2O–NaCl fluids reported by Chou, 1987; Anderko and Pitzer, 1993, and to the data for phonolite–H_2O–Cl system of Signorelli and Carroll,

2000). Furthermore, to our knowledge, there are no literature data on the effect of S on the mixing properties of H_2O–Cl fluids, and the previous experimental studies show no evidence of fluid unmixing in H_2O–S-bearing systems (e.g., Carroll and Webster, 1994). The possible presence of two fluids at experimental conditions is discussed below. Nevertheless, assuming that Cl is mainly incorporated in melt and fluid(s), the mass balance calculation gives the bulk amount of Cl in the fluid phase(s).

4. Results

4.1. Experimental products

At the studied temperature and pressure, all experimental products contain glass, fluid phase, and minerals. The run product glasses are slightly vesicular, and the proportion of vesicles varies in a range of 0.1 to 12.5 vol.%. The vesicularity increases with increasing bulk Cl and S contents, whereas the size of the vesicles increases significantly with increasing bulk Cl (Fig. 1). Most experimental products contain Hb and Pl minerals (Table 3). In some charges, few large Opx are observed (Fig. 1). All S-bearing charges contain Pyr in addition to the three main mineral phases. The dependence of mineral assemblages and proportions of glass and mineral phases on the H_2O, S, and Cl content of the melt is complex. The S-free and Cl-bearing systems usually contain all three main mineral phases (Hb, Opx, and Pl), which are also observed under H_2O-saturated conditions (no S, no Cl, 850 °C, 200 MPa). It must be noted, however, that Hb is not present in the three products of experiments with high added Cl content (Cl-72, ClS-74, and ClS-73), whereas Opx becomes stable. In general, it can be noted that the amount of Opx+Hb decreases, while the proportion of Pl increases with increasing bulk Cl and S concentrations in the system. However, the scattering is very high, and four samples (S-100, ClS-104, ClS-103, and ClS-105) do not contain Pl at all. The proportion of Pyr progressively increases with increasing bulk S.

The total amount of crystals is approximately 10 vol.% at water-saturated conditions in the Cl–S-free system. It slightly decreases with increasing Cl and S content in the melt (note, however, that the relative

proportion of minerals vary, compare plagioclase content in exp. Cl-52 and Cl-72 shown in Fig. 1). It must be noted also that the size of the Hb and Pl increases with Cl concentration in the melt (Cl-51→Cl-52→Cl-72 in Fig. 1), whereas the size of Hb is almost independent on S-content (Cl-51→ClS-79→ClS-80 in Fig. 1). This illustrates that the changing activities of volatiles in the system influence both the phase assemblage and reaction kinetics (crystal nucleation and growth) at given P and T.

4.2. Major-element composition of glasses

The major-element compositions of the glasses are listed in Table 3. The experimental glasses contain less CaO than the starting material as a result of Hb and Pl crystallization. As expected, an increasing amount of added sulfur results in an increase of pyrrhotite content in the experimental products at the expense of FeO$_{tot}$ concentration of the melt (see #Mg, Table 3). For systems with 0.5 wt.% S, the addition of Cl does not affect significantly the FeO$_{tot}$ content of the melt (for systems with less than 0.25 wt.% bulk Cl). The lowest FeO$_{tot}$ contents were found for systems rich in both Cl and S (CIS-75, CIS105, and

CIS-73). The amount of Na$_2$O in the melt decreases slightly with the increasing Cl content in the system, probably due to Pl crystallization and extraction of Na into the fluid phase [formation of Na–Cl-bearing species by the reaction H$^+$(fl)+Na$^+$(m)=Na$^+$(fl)+H$^+$(m)]. However, there is no systematic variation of the degree of peraluminosity with increasing Cl content of the melt (see A/CNK, Table 3).

4.3. H$_2$O, Cl, and S contents of melt and fluid phases

The concentrations of water, chlorine, and sulfur analyzed in the silicate rhyodacitic glasses after the experiments are listed in Table 3 (in wt.%). The CH$_2$O^m (C_i^m=wt.% of component i in the melt) varies in a range of 5.7–7.6 wt.%. The chlorine content of the melt (C_{Cl}^m) shows clearly a positive dependence on the bulk Cl in the system, while the variation of S in the melt (C_S^m) with bulk added sulfur is more complex due to the presence of at least three sulfur-bearing phases. Thus, for the multiphase systems in our experiments, it is more appropriate to investigate the partitioning of volatiles between the different phases. The volatile speciation in the fluid phase is not known in detail. For simplicity, fluid composition

Table 4
The composition of the fluid phase and relationship between Cl and S among phases ($\pm 1\sigma$)

Run number	Cl[a] (mol%)	S[a] (mol%)	H$_2$O[a] (mol%)	Cl^{fl}/Cl^{mb}	S^{fl}/S^{mb}	Cl/S (fl)[b]	Cl/S (m)[b]	Mp S/Mm S[c]	Log fS$_2$[d]
S-100	–	2.9 (1.8)	97.1 (1.8)	–	59	–	–	73	−0.89
S-101	–	7.2 (2.8)	92.8 (2.8)	–	84	–	–	90	−0.92
S-102	–	10.3 (2.8)	89.7 (2.8)	–	108	–	–	133	−1.27
ClS-88	0.3 (0.3)	2.9 (0.9)	96.9 (0.9)	0.4	63	0.1 (0.1)	13 (4)	65	−0.87
Cl-51	1.1 (0.3)	–	98.9 (0.3)	0.6	–	–	–	–	–
ClS-79	1.2 (0.4)	2.2 (2.5)	96.6 (2.6)	0.8	22	0.5 (0.6)	16 (5)	32	−2.30
ClS-80	1.1 (0.4)	2.3 (1.3)	96.7 (1.4)	0.6	18	0.5 (0.3)	13 (3)	59	−2.36
ClS-78	1.3 (0.5)	8.5 (2.8)	90.1 (3.1)	0.9	84	0.2 (0.1)	14 (6)	120	−1.50
Cl-52	1.8 (0.4)	–	98.2 (0.4)	0.5	–	–	–	–	–
ClS-104	3.2 (0.7)	7.1 (1.6)	89.7 (2.0)	1.2	55	0.5 (0.1)	21 (8)	44	−0.92
Cl-53	7.0 (0.9)	–	93.0 (0.9)	1.3	–	–	–	–	–
ClS-103	8.2 (1.3)	3.5 (2.2)	88.3 (2.7)	1.6	30	2.3 (1.5)	43 (22)	19	−1.04
ClS-76	9.8 (2.1)	3.7 (2.0)	86.5 (3.3)	2.4	26	2.6 (1.5)	29 (10)	52	−2.30
ClS-75	8.3 (0.8)	6.2 (1.0)	85.5 (1.6)	2.1	44	1.3 (0.3)	27 (8)	106	−1.58
Cl-72	46.5 (7.1)	–	53.5 (7.1)	6.8	–	–	–	–	–
ClS-74	51.9 (10.2)	5.0 (1.7)	43.0 (11.1)	7.9	35	10.4 (4.1)	45 (17)	20	−2.27
ClS-105	51.7 (13.2)	11.3 (3.3)	37.0 (16.0)	9.3	83	4.6 (1.8)	41 (23)	27	−0.18
ClS-73	43.1 (5.7)	16.9 (3.0)	40.0 (7.9)	8.9	104	2.5 (0.6)	30 (8)	52	−1.88

[a] Concentrations are calculated from mass–balance relationships in experimental products (see text).
[b] Ratios are calculated from molar concentrations of Cl and S in the fluid and melt phases.
[c] Ratio of moles (M) of S incorporated in dense phases [melt (m) and pyrrhotite (p)].
[d] Fugacity of sulfur is calculated from the composition of pyrrhotites using the equation of Toulmin and Barton (1964).
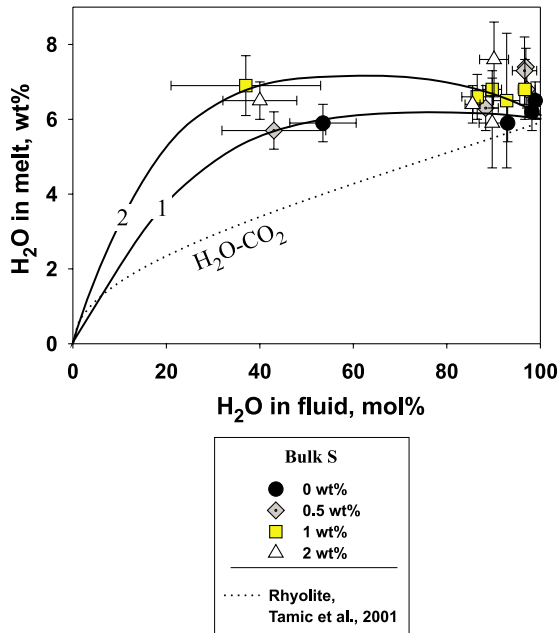
Fig. 2. The relationship between the molar proportion of H_2O in the fluid phase and the H_2O concentration in the silicate melt. Different symbols characterize samples with different bulk content of S as described in the legend; the error bars are 1σ deviations. Dotted line represents the distribution of H_2O between rhyolitic melt and H_2O–CO_2-bearing fluid calculated for given T and P using the model of Tamic et al. (2001). Solid lines are X_{H2O}^{fl} vs. C_{H2O}^m trends of S-poor (1) and S-rich (2) systems. Note that those lines are interpretative and give only qualitative information, however, implying a strong nonideality of the systems.

obtained by mass balance is expressed in terms of mol% of H_2O (X_{H2O}^{fl}), S (X_S^{fl}), and Cl (X_{Cl}^{fl}; Table 4).

The dependence of water solubility in the melt on the H_2O content of the fluid phase is shown in Fig. 2. Despite the fact that determined values have large analytical errors, the data suggest that water solubility in the melt is almost constant, even at low mole fraction of H_2O in the fluid phase (down to 40 mol%). This solubility trend strongly deviates from that of H_2O–CO_2–rhyolite system at same pressure (H_2O solubility vs. X_{H2O}^{fl} is calculated after Tamic et al., 2001, and shown as a dotted line in Fig. 2). The four points in Fig. 2 with the low H_2O contents in the fluid correspond to the samples with the highest bulk Cl contents. We interpret the high water solubility in the melt observed for these samples as due to the nonideality of mixing of Cl-bearing aqueous fluids, as already mentioned by Webster et al. (1999). The

low precision of the analytical technique for H_2O determination does not allow to verify a dependence of C_{H2O}^m on the S content in the system due to the small variation of sulfur content in the fluid (maximum 17 mol% S in fluid, Table 4). However, the higher H_2O melt concentrations in S-rich systems than in S-poor systems suggest that S may enhance slightly melt H_2O solubility in Cl-rich systems (compare solid lines 1 and 2 for S-poor and S-rich systems, respectively).

Fig. 3 shows the Cl concentration in the melt as a function of Cl content in the equilibrium fluid phase. With increasing Cl in the fluid, the solubility of Cl in the melt increases nonlinearly. There is a strong increase of C_{Cl}^m with the first additions of Cl to the system (up to 10 mol% in the fluid) but little changes with further X_{Cl}^{fl} increase. To characterize the Cl-saturated silicate melt, the expected Cl concentration in the melt in equilibrium with a fluid composed only by Cl species (100 mol% Cl) has been calculated using the model of Webster and De Vivo (2002). The obtained value of 1.4 wt.% Cl is assumed to be the maximum Cl content for our rhyodacitic melt at the studied T and P (star in Fig. 3).

The continuous increase of C_{Cl}^m with X_{Cl}^{fl} shown in Fig. 3 suggests that only one fluid phase was present
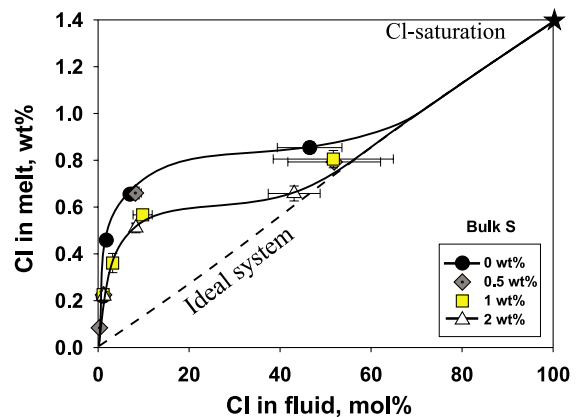

Fig. 3. The solubility of Cl in silicate melt versus Cl content of the fluid phase, where different symbols represent experiments with different amounts of bulk added S as noted in the legend. The error bars are 1σ variations. Solid lines are interpretative representing S-free and S-rich systems. Note that increasing S content of the fluid negatively affects Cl solubility in the melt. The value of Cl-saturation of the rhyodacitic melt (star) is calculated using the model of Webster and De Vivo (2002). The dashed line is assumed to be a Cl distribution between the fluid and the melt in an ideal system.

in the system. If two fluids would have been present (brine and vapor), C_{Cl}^m should be fixed because the Cl activity does not change with X_{Cl}^{fl} (e.g., Carroll and Webster, 1994). On the other hand, the melt composition (see Table 3) and, probably, the relative abundance of species in the complex fluid vary also with the Cl content of the system. Hence, on the basis of our analytical results, it is not possible to exclude fluid immiscibility for intermediate X_{Cl}^{fl}. In any case, the strong nonlinear evolution of C_{Cl}^m with increasing X_{Cl}^{fl} indicates that the conditions are very close to those at which two fluid phases coexist. When compared with the S-free system (at similar mole fraction of Cl in the fluid), the addition of sulfur has a negative effect on the C_{Cl}^m (compare solid lines in Fig. 3). However, for systems with low bulk Cl contents, the effect of S on Cl solubility in the melt cannot be properly resolved.

The solubility of S in the melt as a function of S content of the fluid and bulk Cl in the system is presented in Fig. 4. Although the analytical error of sulfur determination in the melt is high, sulfur solubility shows systematically a small nonlinear positive dependence on S in the fluid. At the same mole fraction of S in the fluid, sulfur concentrations in Cl-bearing melts are higher by up to a factor of two than in Cl-free melts. Even Cl-poor systems show higher S solubilities than Cl-free ones do, indicating
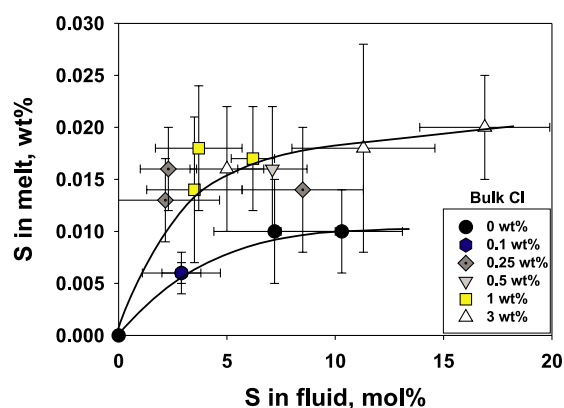
Fig. 4. The solubility of S in silicate melt versus S content of the fluid phase. The symbols are different bulk content of Cl described in the legend. The error bars are 1σ variations. Solid lines are interpretative trends of the evolution of S content of the melt with increasing S in the fluid. Note a systematic increase in S solubility in the melt (up to two times) in Cl-bearing systems.

that, first additions of Cl have an effect on the solubility of S.

4.4. Sulfur fugacity

Sulfur fugacity was calculated from the composition of pyrrhotites, measured by electron microprobe in experimental products, using the equation of Toulmin and Barton (1964). The obtained values are presented in Table 4. Sulfur fugacity in experimental runs varies from $\log fS_2 = -0.18$ to -2.36 and shows no clear dependence on the fluid or system composition. However, it can be noted that there is a large error on sulfur fugacities calculated from the microprobe analyses of pyrrhotite (e.g., as discussed by Whitney, 1984). Thus, the sulfur fugacities given in Table 4 can only be considered as rough estimations.

5. Discussion

5.1. Distribution of H_2O, Cl, and S between fluid and melt

The results given in Tables 3 and 4 and presented in Figs. 2–4 show that the distribution of H_2O, Cl, and S between the fluid and the silicate melt is complex in systems containing multicomponent fluids. All systems are characterized by a deviation from ideal distribution. The high C_{H2O}^m values cannot be explained by changes in melt composition and must be related to high water activities in the fluid. The enhanced water activity in an H–O–Cl-bearing system is not surprising because the properties of the salt-water fluid at studied experimental conditions are expected to be near critical. Due to analytical errors, it is difficult to predict the effect of S on H_2O solubility in Cl-free melts from our data because the variation in X_S^{fl} is too small.

The nonlinear relationship between C_{Cl}^m and X_{Cl}^{fl} (in S-free systems) is consistent with previous results for silicate–salt–H_2O-bearing systems (e.g., Carroll and Webster, 1994; Webster et al., 1999), indicating nonideal mixing in the fluid. The decrease of C_{Cl}^m with increasing X_S^{fl} (at constant X_{Cl}^{fl}) can be explained by an effect of S on the

properties of the fluid phase; that is, an exchange of H–O species in the fluid by S-bearing species decreases the nonideality of mixing. Alternatively, the dissolution of S in the melt and changes in bulk melt composition (e.g., due to Fe depletion) may have a strong influence on the dissolution mechanisms of Cl in silicate melts (as discussed in detail by Webster and De Vivo, 2002).

The nonlinear dependence of C_S^m on X_S^{fl} could be due to the (1) nonideality of mixing in the fluid, (2) changes in the dissolution mechanisms of S in the melt, and/or (3) changes in melt composition. From previous studies, there is no evidence for strong nonideal interactions among H–O–S species (e.g., Carroll and Webster, 1994), and the partition coefficient of sulfur between the fluid and the melt was found to be independent on the S content in Fe-free rhyolite at reduced conditions (Keppler, 1999). Hence, the curvature of the solid line in Fig. 4 is interpreted to be the result of variations in the abundance of S in the system, the speciation of sulfur, and the melt composition (i.e., FeO_{tot} content).

The increase in C_S^m with the addition of small amounts of Cl to the fluid indicates that the distribution of volatiles in Cl-bearing systems may depend significantly not only on the composition of phases but also on the mixing properties of the fluids. Therefore, the interpretation of the solubility of S in the melt as a function of Cl content of the system requires a detailed analysis of both the compositions and properties of volatiles in all coexisting phases (see following sections).

5.2. S and Cl solubilities in melts as a function of H–O–Cl–S fluid composition

The Cl and S solubilities in melts as a function of the H_2O–S–Cl fluid composition are presented in Fig. 5. In this figure, the fluid composition (calculated in mole proportions of Cl, S, and H_2O) is reported on triangular diagrams. The numbers in Fig. 5 (Cl and S) next to each symbol represent the concentrations of Cl and S in the melt in wt.% and ppm, respectively. These concentrations have been used to draw the isopleths of constant Cl and S contents in the melt.

The shape and position of S solubility isopleths are very different from those of Cl (compare Cl and S in Fig. 5). In most of the diagram (part with high Cl concentration in the fluid in Fig. 5 (S)), sulfur solubility increases with increasing sulfur in the fluid. However, it can be noted that, for a given water content in the fluid, a maximum sulfur solubility is observed for a S/Cl ratio in the fluid close to 1 (along the dotted line in Fig. 5 (S)). One further observation is that, for a given S/H_2O in the fluid, sulfur solubility may first increase and then decrease with increasing Cl content in the fluid.

5.3. Effect of mineral proportion and melt composition on chlorine and sulfur distribution

In the case of Cl solubility, the effect of melt composition is supposed to be low because the changes in melt composition are small. From the analysis of the diagrams in Fig. 5, it is obvious that the solubility of Cl in the melt is related neither to the sulfur content of the melt nor to the proportion of pyrrhotite nor to the FeO_{tot} concentration (compare shape and position of isopleths). Thus, we conclude that the C_{Cl}^m is mainly controlled by the composition of the fluid phase(s). Because pyrrhotite is always present in the S-bearing experimental products, the crystallization of pyrrhotite must influence the partitioning of S between the melt and the fluid due to changes in the melt and/or fluid composition (Scaillet et al., 1998). The analysis of BSE images indicates that the amount of pyrrhotite varies in the experimental products with Cl, S, and H_2O contents in the fluid (from 0 to 2.2 vol.% of the condensed phases; Fig. 5 (Pyr)). The shape of the isopleths for constant amount of pyrrhotite (curves in Fig. 5 (Pyr)) is similar to the shape of the curves for constant sulfur content of the melt (compare S and Pyr in Fig. 5). The increase of pyrrhotite content in the charge is related, in turn, to a decrease of FeO_{tot} content in the coexisting melt, as illustrated in Fig. 5 (FeO; see also Table 3). Thus, the increase in sulfur solubility could be simply due to a decrease in FeO_{tot}. Such a negative correlation between C_S^m and FeO_{tot} was observed in dry mafic systems with FeO_{tot} up to
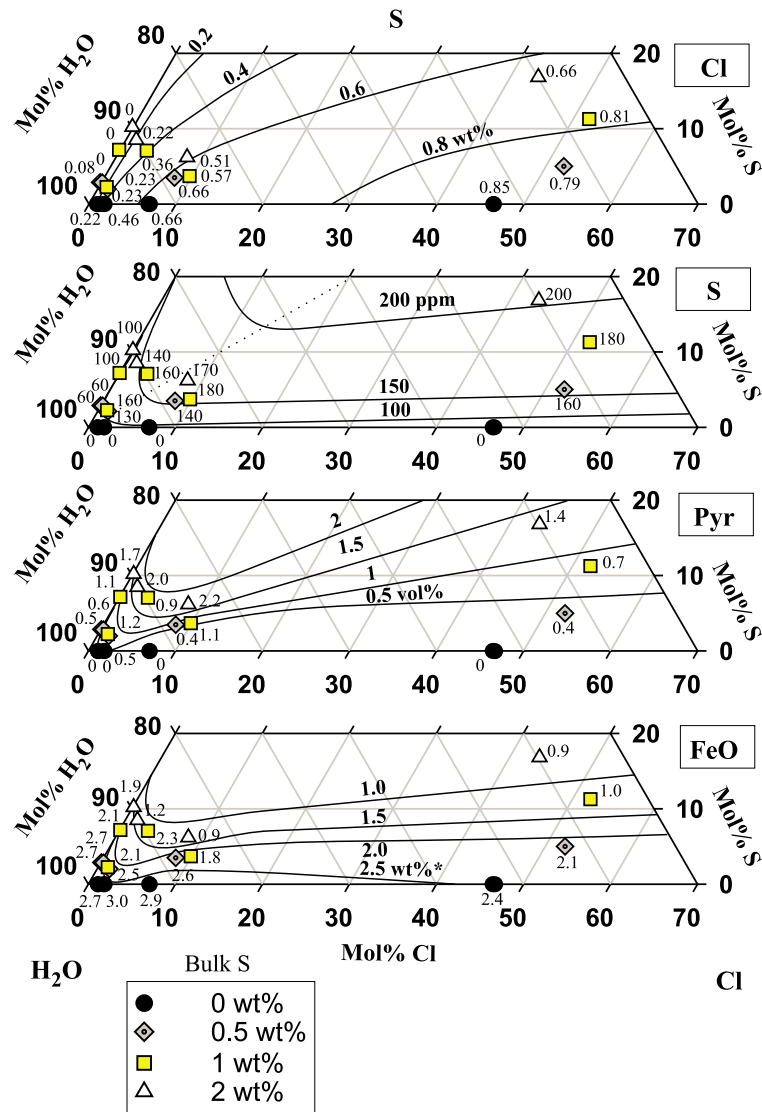
Fig. 5. Triangular plots of the solubilities of chlorine (Cl) and sulfur (S) in the melt, the proportion of crystallized pyrrhotite (Pyr), and the concentration of FeO$_{tot}$ (FeO) in the melt as a function of mixed fluid (H$_2$O–Cl–S) composition on the molar basis. The numbers shown close to data points are Cl, S, and FeO$_{tot}$ concentrations in the melt (wt.%, ppm, normalized wt.%*, respectively) and Pyr proportions (vol.%). Solid lines represent estimated isopleths of component concentrations in the melt or proportion in the system. Different symbols are different bulk S content. The dotted line in the diagram (S) is fluid composition with Cl/S molar ratio equal to 1.

4–6 wt.% (e.g., O'Neil and Mavrogenes, 2002). However, FeO$_{tot}$ is not the only factor controlling C_S^m because, at constant FeO$_{tot}$, the sulfur solubility is systematically higher in Cl-bearing than in Cl-free melts (Fig. 6). Thus, an additional factor needs to be considered to explain the variation in sulfur solubility.

5.4. Mixing properties of the fluid phase as a factor controlling Cl and S solubility

It is well known that H$_2$O–(Na,K)Cl fluids show a strong tendency for unmixing with activity coefficients ≫1 for H$_2$O, NaCl, and KCl (e.g., Chou, 1987; Anderko and Pitzer, 1993). Adding
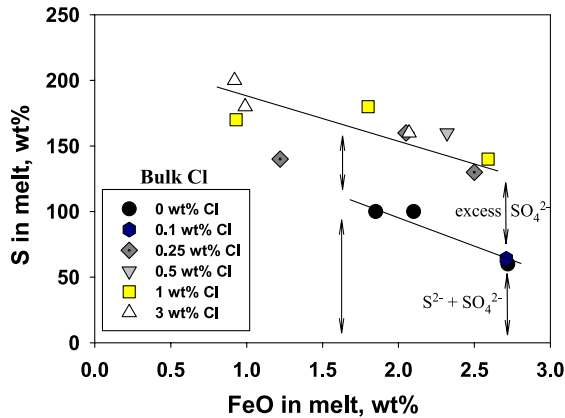
Fig. 6. The relationship between S solubility and FeO$_{tot}$ concentration in the melt. The error bars for S contents of the melt are shown in Fig. 4, whereas the maximum error for FeO$_{tot}$ concentrations is about 0.3 wt.% (see Table 3). Although all trends are negative, Cl-bearing melts show strong enrichment in S even at the same FeO$_{tot}$ content. Arrows show the relative proportions of sulfide (S^{2-}) and sulfate (SO$_4^{2-}$) sulfur species dissolved in the melt.

CO$_2$ to the system increases the nonideality of mixing, and the activity coefficients for H$_2$O and alkali chlorides grow (e.g., Joyce and Holloway, 1993; Duan et al., 1995, 2003; Shmulovich et al., 1995; Shmulovich and Graham, 2004). Our results indicate that the effect on the activities of fluid components is different when sulfur is added instead of CO$_2$. Changes in the concentrations of dissolved species in the coexisting silicate melt suggest that the addition of S may increase slightly the water activity in Cl-rich fluids (Fig. 2) but, in contrast to carbon dioxide, decreases the activity of Cl-bearing species (Fig. 3). The different behavior can be rationalized by considering the speciation of carbon and sulfur in the fluid. At relatively oxidizing conditions, as in our experiments, CO$_2$ is the most abundant carbon species (e.g., Holloway and Blank, 1994; Tamic et al., 2001; Churakov and Gottschalk, 2003). Other carbon species (e.g., CO and CH$_4$) with relative abundance of a few percent or less are of minor importance. SO$_2$ and H$_2$S are the dominant sulfur species in fluids equilibrated with pyrrhotite-bearing magmas (Whitney, 1984) and the most important redox components in volcanic gases (so-called "sulfur buffer", Giggenbach, 1987) and, possibly, in magmatic systems (Matthews et al., 1994). The SO$_2$–H$_2$S equilibrium

depends on water activity, as well as on hydrogen (or oxygen) fugacity

$$H_2S + 2H_2O = SO_2 + 3H_2 \tag{1}$$
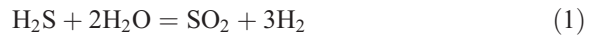
CO$_2$ is a linear molecule without a permanent dipole moment and has a low potential to stabilize ions in fluids. On the other hand, both H$_2$S and SO$_2$ have permanent dipole moments and, hence, are much better suited to complex with ions such as Cl$^-$ and Na$^+$ in dense fluids. Therefore, the tendency for mixing of H$_2$O–Cl fluids decreases when sulfur is added but increases when carbon is added.

The nonideality of mixing in the fluid can explain, in general, the higher sulfur solubilities in silicate melts in Cl-bearing systems than in Cl-free systems. However, if sulfur is dissolved exclusively as sulfide, it can be expected that the sulfur solubility is limited by the concentration of FeO$_{tot}$ in the melt due to the formation of pyrrhotite. The higher concentrations of S in Cl-bearing compared with Cl-free melts at constant FeO$_{tot}$ (see Fig. 6) indicate that other S species must be present in the melt besides sulfide.

### 5.5. Possible factors controlling sulfur solubility in the melt

Sulfur can be dissolved in silicate melts in form of at least two species, sulfide and sulfate (e.g., Carroll and Webster, 1994). The relative abundance of species depends strongly on oxygen fugacity

$$S^{2-}(m) + 2O_2(fl) = SO_4^{2-}(m) \tag{2}$$
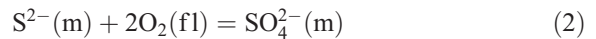
In hydrous systems, H$_2$O serves as a source and H$_2$ as a sink for oxygen according to the reaction

$$H_2O = H_2 + 1/2O_2 \tag{3}$$

In this case, the dissolution mechanisms for sulfur can be described by the following reactions (e.g., Burnham, 1979)

$$H_2S(fl) + O^{2-}(m) = H_2O(fl) + S^{2-}(m) \tag{4}$$

$$SO_2(fl) + O^{2-}(m) + 1/2O_2(fl) = SO_4^{2-}(m) \tag{5}$$
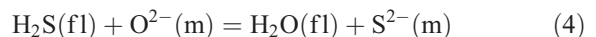
Spectroscopic studies indicate that S^{2-} is bound to tetrahedral cations and plays a similar role as nonbridging oxygens (Asahi et al., 2003). In contrast,

SO_4^{2-} is incorporated on interstitial sites similar to other large incompatible anions such as Cl^{-1} (Tsujimura et al., 2003; Stebbins and Du, 2003).

At $\log fO_2 < NNO$, the solubility of sulfur is strongly dependent on melt FeO content (Haughton et al., 1974; Katsura and Nagashima, 1974; Wendlandt, 1982; Carroll and Rutherford, 1985, 1987; Luhr, 1990; O'Neil and Mavrogenes, 2002) due to the formation of pyrrhotite

$$H_2S(fl) + FeO(m) = FeS(pyr) + H_2O(fl) \qquad (6)$$

Reactions (4) and (6) can explain the increase in sulfur content with decreasing FeO_{tot} for the chlorine-free system but not the increase of sulfur solubility with the addition of chlorine at constant FeO_{tot} content of the melt (Fig. 6).

The transition from sulfide to sulfate being the dominant sulfur species in the melt is close to NNO oxygen buffer (e.g., Carroll and Webster, 1994; Moretti et al., 2003). Although NNO is used as an oxygen buffer in the autoclave, the oxygen fugacity in the experimental capsules varies as a function of the fugacities of volatile species involved in redox reactions because the capsule wall is permeable to hydrogen and not to oxygen. According to the reactions (1) and (3), the increase in H_2O fugacity when adding Cl imposes an increase of fO_2 and SO_2/H_2S ratio because fH_2 was fixed in the experiments. In other words, the addition of Cl to S-bearing systems will shift the redox conditions to more oxidized. Our results do not allow to calculate the exact fugacities of all volatile species, and the variations of the redox states cannot be estimated quantitatively. Nevertheless, at the studied redox conditions, small differences in fO_2 may have a large effect on sulfur speciation because the transition from sulfide to sulfate stability occurs over an fO_2 interval of only two log units.

Following the discussion above, the difference in S content of Cl-free and Cl-bearing systems could be interpreted as the "excess" sulfate content of the melt (note, however, that SO_4^{2-} can be also present as a minor component in the Cl-free system at studied redox conditions). However, fugacities of volatiles and speciation of S and Fe in the melt need to be constrained to interpret quantitatively the distribution of Cl and S between the melt and the fluid(s).

Another possibility to explain the "excess" sulfur in Cl-bearing systems is that sulfur and chlorine form S–Cl-bearing complexes in the melt. The reaction can be written as

$$S^{2-} + xCl^- = [S - Cl_x]^{(2+x)-} \qquad (7)$$
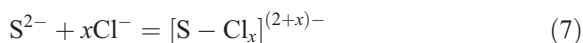
The formation of S–Cl-bearing complexes in the melt should increase the total solubility of both components in the silicate melt. Because the solubility of Cl is two orders of magnitude higher than that of S, the relative increase in solubility is expected to be much larger for S than for Cl. However, S–Cl components usually are unstable in the presence of water (e.g., reaction $SCl_2 + H_2O = 2HCl + SO_2$) and, hence, it is unlikely that S–Cl complexes can exist in hydrous silicate melts.

5.6. Implications for Cl and S contents in fluid-bearing magmatic systems

Our results can be used to estimate the composition, and especially the Cl/S ratio, of fluids coexisting with melts if the Cl/S ratio of the melt is known (e.g., the volatile contents of melts prior to eruption can be constrained using glass inclusions in minerals). As shown in Fig. 7, the molar Cl/S ratio in fluids coexisting with melts is much lower than that of the melt. Hence, sulfur is partitioned
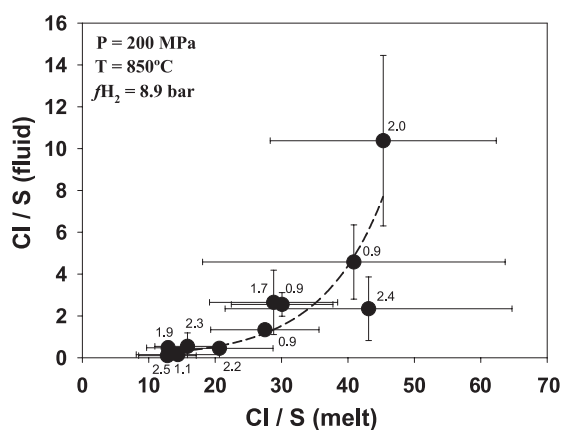

Fig. 7. The ratio of molar Cl and S concentrations in the fluid versus the molar ratio of Cl and S concentrations in the melt. The dashed line is an exponential function for the data. Numbers represent FeO_{tot} concentrations (wt.%) in the melt.

preferentially into the fluid phase compared with Cl, as expected from studies on solubilities of H–O–Cl and H–O–S fluids in melts. This has implications on the evolution of degassing magma. The first exsolved fluids will have high S contents, but the Cl/S ratio in the fluid will increase with ongoing magma degassing. However, this scenario is valid only in absence of S-bearing crystalline phases (pyrrhotite and/or anhydrite), which can buffer the concentration of S in the melt. In our experiments, the amount of S incorporated in pyrrhotite is 20–120 times larger than that in the melt, although pyrrhotite is only a minor phase (see Table 3), as illustrated in Fig. 8. This supports the idea that pyrrhotite may exert a strong control on the budget of S in magmatic systems as suggested by Scaillet et al. (1998).

The relationship between Cl/S (fluid) and Cl/S (melt) is nearly exponential (dashed line in Fig. 7) due to the strongly nonideal behavior of Cl-bearing fluids. Therefore, the Cl/S ratio in the fluid can be predicted only at low values of Cl/S (melt), but not at high values (>40), because of the large variation of Cl/S (fluid) with Cl/S (melt) in the later case. A relationship between Cl and S fluid/melt partitioning and FeO$_{tot}$ is not evident from our data (see numbers
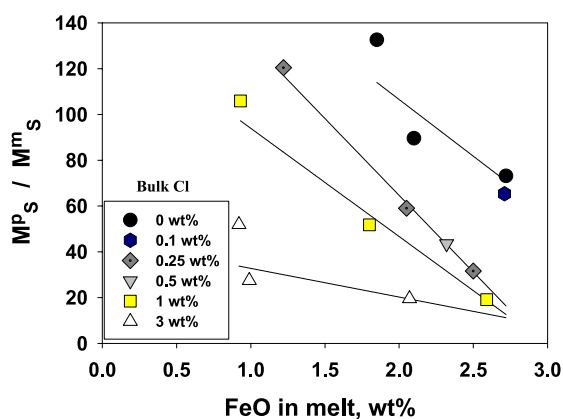

Fig. 8. The M_S^g/M_S^m ratio [=(mole of sulfur in pyrrhotite)/(mole of sulfur in melt)] versus FeO$_{tot}$ content of the melt. Lines show trends with similar bulk concentrations of Cl in the system. Increasing Cl in the system favors S distribution between dense phases in respect to melt. Remarkable is the high proportion of S incorporated into the pyrrhotite (which is a minor phase in the system), indicating that the presence of pyrrhotite affects significantly the budget of S in magmatic system.

close to the symbols in Fig. 7). However, it can be expected that changes in the hydrogen fugacity will shift the partitioning curve. Assuming constant total iron in the melt, an increase in fH$_2$ will produce a higher proportion of ferrous iron in the melt and, hence, it will reduce the solubility of sulfide (see reaction (6)). Furthermore, the concentration of dissolved sulfate is expected to be lower at more reducing conditions. Thus, the curve in Fig. 7 will be shifted to the right. However, if the total iron in the melt decreases due to the formation of pyrrhotite, the sulfide solubility will increase and compensate the effect of increasing fH$_2$.

The Cl/S ratios in fluids can vary significantly in volcanic systems (e.g., Symonds et al., 1994; Edmonds et al., 2001; Aiuppa et al., 2002), and the Cl/S solubility ratios need to be determined to model magma degassing (e.g., Aiuppa et al., 2002). The data obtained in this study represent a first attempt to determine such solubility ratios. Because of the nonideality of Cl-bearing fluids in the investigated P-T-X range, the application of the data is restricted to dacitic compositions (similar to Unzen dacite, Nakada and Motomura, 1999) and P-T-fO$_2$ conditions close to 200 MPa, 850 °C, and NNO. In the case of Unzen volcano, the Cl/S molar ratio in the mixed magma prior to eruption is estimated to be about 6–10 using the data on S contents in glass inclusions (Satoh et al., 2003) and Cl partitioning data between amphibole and melt (Sato et al., in press). In the matrix glass of the eruptive products, Cl/S is about 11–15 (according to the data of Yamaguchi, 1997, considering an S content of 50 ppm). From Fig. 7, the estimated Cl/S ratios in the fluid with Cl/S in the melt between 6 and 15 should be below 1. This is consistent with the Cl/S ratio of 0.2–0.5 determined in volcanic gases of Unzen (Mori et al., 1993; Ohba et al., 1994).

Another example that can be discussed on the basis of our experimental data is the Soufrière Hills volcano (Montserrat), which has similar eruption style, magma storage conditions, and melt compositions than Unzen volcano (e.g., Barclay et al., 1998; Devine et al., 1998, 2003; Rutherford and Devine, 2003). In this case, Cl/S variations in fluids and melts are much more significant (Edmonds et al., 2001). The Cl/S ratio in volcanic gases ranges from 0.3 to 3.6 (calculated from HCl/SO$_2$ ratio only; Cl/S$_{total}$

ratios are lower because of additional H_2S). Glass inclusions and matrix glass show a broad range of Cl/ S values from 3 to 65. The Cl/S fractionation trend in Fig. 7 indicates that large variations of Cl/S in fluid can be expected for the determined Cl/S in melts. However, the excess sulfur problem still remains unsolved in the case of Soufrière Hills volcano (Edmonds et al., 2001) because the Cl/S ratio in fluids is much lower than expected from Cl/S values for the melt.

6. Conclusions

Our new results indicate that the solubilities of Cl and H_2O in rhyodacitic melts are mainly controlled by the activities of volatiles, which, in turn, are strongly influenced by the mixing properties of the fluid phase at given P and T. At magmatic conditions, the interaction between Cl-bearing fluid species is strong, resulting in enhanced activity coefficients of species and favoring a tendency of fluid immiscibility. Thus, the solubilities of both Cl and H_2O in the silicate melt can increase with the addition of Cl to the system. Remarkable is that the addition of S to the system decreases the solubility of Cl. Thus, S-bearing species reduce (in contrast to CO_2) the nonideality of the Cl-bearing aqueous fluid.

On the other hand, the solubility of S in the melt is a complex function of fluid composition, the FeO_{tot} content of the melt, and, finally, the speciation of S in the melt. The addition of Cl enhances S solubility up to two times due to (1) the increase in activity coefficients of S-bearing fluid species and (2) the "oxidizing" effect of Cl on the fH_2-buffered system caused by an increase in water fugacity. The first factor results in a higher solubility of sulfide in the melt, an increase of the amount of crystallized pyrrhotite, and a depletion of FeO_{tot} in the melt. The second factor favors the dissolution of S as additional sulfate in the melt.

These observations emphasize the complexity of the fluid–melt–mineral systems containing multicomponent volatiles. Thus, an application of results obtained in simple systems, containing single or binary fluids, to model natural processes (i.e., magma degassing) should be treated with caution.

References

Aiuppa, A., Federico, C., Paonita, A., Pecoraino, G., Valenza, M., 2002. S, Cl and F degassing as an indicator of volcanic dynamics: the 2001 eruption of Mount Etna. Geophys. Res. Lett. 29, 54.

Anderko, A., Pitzer, K.S., 1993. Equation-of-state representation of phase equilibria and volumetric properties of the system NaCl–H_2O above 573 K. Geochim. Cosmochim. Acta 57, 1657–1680.

Asahi, T., Miura, Y., Yamashita, H., Aekawa, T., 2003. Local structure analysis of alkali silicate glasses containing sulfur. Geochim. Cosmochim. Acta 67, 18(S1), A26.

Barclay, J., Rutherford, M.J., Carroll, M.R., Murphy, M.D., Devine, J.D., Gardner, J.E., Sparks, R.S.J., 1998. Experimental phase equilibria constraints on the pre-eruptive storage conditions of the Soufrière Hills magma. Geophys. Res. Lett. 25, 3437–3440.

Behrens, H., Ohlhorst, S., Holtz, F., Champenois, M., 2004. CO_2 solubility in dacitic melts equilibrated with H_2O–CO_2 fluids—implications for modelling the solubility of CO_2 in silicic melts. Geochim. Cosmochim. Acta (in press).

Burnham, C.W., 1979. Magmas and hydrothermal fluids. In: Barns, H.L. (Ed.), Geochem. Hydrotherm. Ore Dep. John Willey & Sons, New York, pp. 34–76.

Carroll, M.R., Rutherford, M.J., 1985. Sulfide and sulfate saturation in hydrous silicate melts. J. Geophys. Res. 90, 601–612.

Carroll, M.R., Rutherford, M.J., 1987. The stability of igneous anhydrite: experimental results and implications for sulfur behavior in the 1982 El Chichon trachyandesite and other evolved magmas. J. Petrol. 28, 781–801.

Carroll, M.R., Rutherford, M.J., 1988. Sulfur speciation in hydrous experimental glasses of varying oxidation state: results from measured wavelength shifts of sulfur X-rays. Am. Mineral. 73, 845–849.

Carroll, M.R., Webster, J.D., 1994. Solubilities of sulfur, noble gases, nitrogen, chlorine, and fluorine in magmas. In: Carroll, M.R., Holloway, J.R. (Eds.), Volatiles in Magmas, Rev. Mineral., vol. 30. Mineral. Soc. Am., Washington, pp. 231–280.

Chou, I.-M., 1987. Phase relations in the system NaCl–KCl–H_2O: III. Solubilities of halite in vaporsaturated liquids above 445 °C and redetermination of phase equilibrium properties in the

system NaCl–H$_2$O to 1000 °C and 1500 bars. Geochim. Cosmochim. Acta 51, 1965–1975.

Churakov, S., Gottschalk, M., 2003. Perturbation theory based equation of state for polar molecular fluids: II. Fluid mixtures. Geochim. Cosmochim. Acta 67, 2415–2425.

Davis, M.G., Garcia, M.O., Wallace, P., 2003. Volatiles in glasses from Mauna Loa Volcano, Hawai'I: implications for magma degassing and contamination, and growth of Hawaiian volcanoes. Contrib. Mineral. Petrol. 144, 570–591.

Deer, W.A., Howie, R.A., Zussman, J., 1992. An Introduction to the Rock-Forming Minerals. 2nd ed. Longman, Hong Kong.

De Hoog, J.C.M., Koetsier, G.W., Bronto, S., Sriwana, T., van Bergen, M.J., 2001. Sulfur and chlorine degassing from primitive arc magmas: temporal changes during the 1982–1983 eruptions of Galunggung (West Java, Indonesia). J. Volcanol. Geotherm. Res. 108, 55–83.

Devine, J.D., Gardner, J.E., Brack, H.P., Layne, G.D., Rutherford, M.J., 1995. Comparison of microanalytical methods for estimating H$_2$O contents of silicic volcanic glasses. Am. Mineral. 80, 319–328.

Devine, J.D., Myrphy, M.D., Rutherford, M.J., 1998. Petrologic evidence for pre-eruptive pressure-temperature conditions, and recent reheating, of andesitic magma erupting at the Soufrière Hills Volcano, Montserrat, WI. Geophys. Res. Lett. 25, 3669–3672.

Devine, J.D., Rutherford, M.J., Norton, G.E., Young, S.R., 2003. Magma storage region processes inferred from geochemistry of the Fe–Ti oxides in andesitic magma, Soufrière Hills Volcano, Montserrat, WI. J. Petrol. 44, 1375–1400.

Duan, Z., Moeller, N., Weare, J.H., 1995. Equation of state for the NaCl–H$_2$O–CO$_2$ system: prediction of phase equilibria and volumetric properties. Geochim. Cosmochim. Acta 59, 2869–2882.

Duan, Z., Moeller, N., Weare, J.H., 2003. Equations of state for the NaCl–H$_2$O–CH$_4$ system and the NaCl–H$_2$O–CO$_2$–CH$_4$ system: phase equilibria and volumetric properties above 573 K. Geochim. Cosmochim. Acta 67, 671–680.

Edmonds, M., Pyle, D., Oppenheimer, C., 2001. A model for degassing at the Soufriere Hills volcano, Montserrat, West Indies, based on geochemical data. Earth Planet. Sci. Lett. 186, 159–173.

Francis, P., Maciejewski, A., Oppenheimer, C., Chaffin, C., Caltabiano, T., 1995. SO$_2$:HCl ratios in the plumes from Mt. Etna and Volcano determined by Fourier Transform Spectroscopy. Geophys. Res. Lett. 22, 1717–1720.

Giggenbach, W.F., 1987. Redox processes governing the chemistry of fumarolic gas discharges from White Island, New Zealand. Appl. Geochem. 2, 143–161.

Giggenbach, W.F., 1996. Chemical composition of volcanic gases. In: Scarpa/Tilling (Ed.), Monitoring and Mitigation of Volcanic Hazards. Springer, Berlin, pp. 221–256.

Harms, E., Schmincke, H.-U., 2000. Volatile composition of the phonolitic Laacher See magma (12,900 yr BP): implications for syn-eruptive degassing of S, F, Cl and H$_2$O. Contrib. Mineral. Petrol. 138, 84–98.

Haughton, D.R., Roeder, P.L., Skinner, B.J., 1974. Solubility of sulfur in mafic magmas. Econ. Geol. 69, 451–467.

Holloway, J.R., Blank, J.G., 1994. Application of experimental results to C–O–H species in natural melts. In: Carroll, M.R., Holloway, J.R. (Eds.), Volatiles in Magmas, Rev. Mineral., vol. 30. Mineral. Soc. Am., Washington, pp. 187–230.

Holtz, F., Sato, H., Lewis, J., Behrens, H., Nakada, S., 2004. Experimental petrology of the 1991–1995 Unzen dacite: Part I. Phase relations, phase composition and pre-eruptive conditions. J. Petrol. (in press).

Joyce, D.B., Holloway, J.R., 1993. An experimental determination of the thermodynamic properties of H$_2$O–CO$_2$–NaCl fluids at high pressures and temperatures. Geochim. Cosmochim. Acta 57, 733–746.

Katsura, T., Nagashima, S., 1974. Solubility of sulfur in some magmas at 1 atmosphere. Geochim. Cosmochim. Acta 38, 517–531.

Keppler, H., 1999. Experimental evidence for the source of excess sulfur in explosive volcanic eruptions. Science 284, 1652–1654.

Luhr, J.F., 1990. Experimental phase relations of water- and sulfur-saturated arc magmas and the 1982 eruptions of El Chichon volcano. J. Petrol. 31, 1071–1114.

Malinin, S.D., Kravchuk, I.F., Delbove, F., 1989. Chloride distribution between phases in hydrated and dry chloride–aluminosilicate melt systems as a function of phase composition. Geochem. Int. 26, 32–38.

Matthews, S.J., Jones, A.P., Beard, A.D., 1994. Buffering of melt oxygen fugacity by sulfur redox reactions in calc-alkaline magmas. J. Geol. Soc. (Lond.) 151, 815–823.

Metrich, N., Rutherford, M.J., 1992. Experimental study of chlorine behavior in hydrous silicic melts. Geochim. Cosmochim. Acta 56, 607–616.

Metrich, N., Clocchiatti, R., Mosbah, M., Chaussidon, M., 1993. The 1989–1990 activity of Etna magma mingling and ascent of H$_2$O–Cl–S-rich basaltic magma-evidence from melt inclusions. J. Volcanol. Geotherm. Res. 59 (1–2), 131–144.

Mori, T., Notsu, K., 1997. Remote CO, COS, CO$_2$, SO$_2$ and HCl detection and temperature estimation of volcanic gas. Geophys. Res. Lett. 24, 2047–2050.

Mori, T., Notsu, K., Tohjima, Y., Wakita, H., 1993. Remote detection of HCl and SO$_2$ in volcanic gas from Unzen volcano, Japan. Geophys. Res. Lett. 20, 1355–1358.

Moretti, R., Papale, P., Ottonello, G., 2003. A model for the saturation of C–O–H–S fluids in silicate melts. In: Oppenheimer, C., Pyle, D.M., Barclay, J. (Eds.), Volcanic Degassing, Special Pub.-Geol. Soc. London, vol. 213, pp. 81–101.

Nakada, S., Motomura, Y., 1999. Petrology of the 1991–1995 eruption at Unzen: effusion pulsation and groundmass crystallization. J. Volcanol. Geotherm. Res. 89, 173–196.

Ohba, T., Hirabayashi, J., Yoshida, M., 1994. Equilibrium temperature and redox state of volcanic gas at Unzen volcano, Japan. J. Volcanol. Geotherm. Res. 60, 263–272.

O'Neil, H.S.C., Mavrogenes, J.A., 2002. The sulfide capacity and the sulfur content at sulfide saturation of silicate melts at 1400 °C and 1 bar. J. Petrol. 43, 1049–1087.

Rutherford, M.J., Devine, J.D., 2003. Magmatic conditions and magma ascent as induced by hornblende phase equilibria and reactions in the 1995–2002 Soufrière Hills magma. J. Petrol. 44, 1433–1454.

Sato, H., Nakada, S., Fujii, T., Nakamura, M., Suzuki-Kamata, K., 1999. Groundmass pargasite in the 1991–1995 dacite of Unzen volcano: phase stability experiments and volcanological implications. J. Volcanol. Geotherm. Res. 89, 197–212.

Sato, H., Holtz, F., Behrens, H., Botcharnikov, R.E., Nakada, S., 2004. Experimental petrology of the 1991–1995 dacite of Unzen volcano: Part II. Cl/OH partitioning between hornblende and melt and its implications for the origin of oscillatory zoning of hornblende phenocryst. J. Petrol. (n press).

Satoh, H., Saito, G., Shinohara, H., Yamaguchi, Y., 2003. Sulfur source for the 1991–1995 Unzen eruption: evidence from melt inclusions in pyroxenes. Geophys. Res. Lett. 30, 2220.

Scaillet, B., Pichavant, M., 2003. Experimental constraints on volatile abundances in arc magmas and their implications for degassing processes. In: Oppenheimer, C., Pyle, D.M., Barclay, J. (Eds.), Volcanic Degassing, Special Pub.-Geol. Soc. London, vol. 213, pp. 23–52.

Scaillet, B., Clemente, B., Evans, B.W., Pichavant, M., 1998. Redox control of sulfur degassing in silicic magmas. J. Geophys. Res. 103, 23937–23949.

Self, S., King, A.J., 1996. Petrology and sulfur and chlorine emissions of the 1963 eruption of Gunung Agung, Bali, Indonesia. Bull. Volcanol. 58, 263–285.

Shinohara, H., Iiyama, J.T., Matsuo, S., 1989. Partition of Cl between silicate melt and hydrothermal solutions: I. Partition of NaCl–KCl. Geochim. Cosmochim. Acta 53, 2617–2630.

Shmulovich, K.I., Graham, C.M., 2004. An experimental study of phase equilibria in the systems H_2O–CO_2–$CaCl_2$ and H_2O–CO_2–NaCl at high pressures and temperatures (500–800 °C, 0.5–0.9 GPa): geological and geophysical applications. Contrib. Mineral. Petrol. 146, 450–462.

Shmulovich, K.I., Tkachenko, S.I., Plyasunova, N.V., 1995. Phase equilibria in fluid systems at high pressures and temperatures. In: Shmulovich, K.I., Yardley, B.W.D., Gonchar, G.G. (Eds.), Fluids in the Crust. Chapman and Hall, London, pp. 193–214.

Signorelli, S., Carroll, M.R., 2000. Solubility and fluid-melt partitioning of Cl in hydrous phonolitic melts. Geochim. Cosmochim. Acta 64, 2851–2862.

Stebbins, J.F., Du, L.-S., 2003. Chloride ion sites in silicate and aluminosilicate glasses: a preliminary study by [35]Cl solid-state NMR. Am. Mineral. 87, 359–363.

Symonds, R.B., Rose, W.I., Bluth, G.J.S., Gerlach, T.M., 1994. Volcanic-gas studies: methods, results and applications. In: Carroll, M.R., Holloway, J.R. (Eds.), Volatiles in Magmas, Rev. Mineral., vol. 30. Mineral. Soc. Am., Washington, pp. 1–66.

Tamic, N., Behrens, H., Holtz, F., 2001. The solubility of H_2O and CO_2 in rhyolitic melts in equilibrium with a mixed CO_2–H_2O fluid phase. Chem. Geol. 174, 333–347.

Thordarson, Th., Self, S., Oskarson, N., Hulsebosch, T., 1996. Sulfur, chlorine, and fluorine degassing and atmospheric loading by the 1783–1784 AD Laki (Skaftar Fires) eruption in Iceland. Bull. Volcanol. 58, 205–225.

Toulmin, P., Barton Jr., P.B., 1964. A thermodynamic study of pyrite and pyrrhotite. Geochim. Cosmochim. Acta 28, 641–671.

Tsujimura, T., Xue, X., Walter, M.J., Yamashita, S., Kanzaki, M., 2003. The effect of sulfate sulfur on the structure of Na_2O–SiO_2 glasses: a ^{29}Si MAS NMR, Raman and FTIR study. Geochim. Cosmochim. Acta 67, 18(S1), A494.

Venezky, D.Y., Rutherford, M.J., 1999. Petrology and Fe–Ti oxide reequilibration of the 1991 Mount Unzen mixed magma. J. Volcanol. Geotherm. Res 89, 213–230.

Webster, J.D., 1992. Fluid-melt interactions involving Cl-rich granites: experimental study from 2 to 8 kbar. Geochim. Cosmochim. Acta 56, 659–678.

Webster, J.D., 1997. Chloride solubility in felsic melts and the role of chloride in magmatic degassing. J. Petrol. 38, 1793–1807.

Webster, J.D., De Vivo, B., 2002. Experimental and modeled solubilities of chlorine in aluminosilicate melts, consequences of magma evolution, and implications for exsolution of hydrous chloride melt at Mt. Somma-Vesuvius. Am. Mineral. 87, 1046–1061.

Webster, J.D., Holloway, J.R., 1988. Experimental constraints on the partitioning of Cl between topaz rhyolite melt and H_2O and H_2O+CO_2 fluids: new implications for granitic differentiation and ore deposition. Geochim. Cosmochim. Acta 52, 2091–2105.

Webster, J.D., Kinzler, R.J., Mathez, E.A., 1999. Chloride and water solubility in basalt and andesite liquids and implications for magmatic degassing. Geochim. Cosmochim. Acta 63, 729–738.

Webster, J.D., Raia, F., DeVivo, B., Rolandi, G., 2001. The behavior of chlorine and sulfur during differentiation of the Mt. Somma-Vesuvius magmatic system. Mineral. Petrol. 73, 177–200.

Wendlandt, R.F., 1982. Sulfide saturation of basalt and andesite melts at high pressure an temperature. Am. Mineral. 67, 877–885.

Whitney, J.A., 1984. Fugacities of sulfurous gases in pyrrhotite-bearing silicic magmas. Am. Mineral. 69, 69–78.

Yamaguchi, Y., 1997. Chlorine, sulfur and fluorine contents of melt inclusions in phenocrysts, matrix glass, and cryptocrystalline phases in dacites of the 1991 eruption, Unzen volcano. Proc. Unzen, pp. 117–119.